Crystal structure of human stem cell factor: Implication for stem cell factor receptor dimerization and activation

Zhongtao Zhang*, Rongguang Zhang†, Andrzej Joachimiak†, Joseph Schlessinger*‡¶, and Xiang-Peng Kong‡§¶

Departments of *Pharmacology and §Biochemistry and ‡Skirball Institute, New York University School of Medicine, 550 First Avenue, New York, NY 10016; and †Argonne National Laboratory, Argonne, IL 60439

Contributed by Joseph Schlessinger, May 17, 2000

Stem cell factor (SCF) plays important roles in hematopoiesis and the survival, proliferation, and differentiation of mast cells, melanocytes, and germ cells. SCF mediates its biological effects by binding to and activating a receptor tyrosine kinase designated c-kit or SCF receptor. In this report we describe the 2.3-Å crystal structure of the functional core of recombinant human SCF. SCF is a noncovalent homodimer composed of two slightly wedged protomers. Each SCF protomer exhibits an antiparallel four-helix bundle fold. Dimerization is mediated by extensive polar and nonpolar interactions between the two protomers with a large buried surface area. Finally, we have identified a hydrophobic crevice and a charged region at the tail of each protomer that functions as a potential receptor-binding site. On the basis of these observations, a model for SCF·c-kit complex formation and dimerization is proposed.

Stem cell factor (SCF) is a growth factor that stimulates the survival, proliferation, and differentiation of hematopoietic cells. SCF is critical for mast cell production and function and plays an important role in the development of melanocytes, germ cells, and intestinal pacemaker cells (1). SCF is also known as mast cell growth factor (MCGF) (2), *steel* (*Sl*) factor (SLF) (3), or kit ligand (KL) (4), and it elicits its biological functions by binding to and activating a cell surface receptor designated c-kit or SCF receptor (SCFR). c-kit belongs to the type III receptor tyrosine kinase (RTK) subfamily, whose members include platelet-derived growth factor (PDGF) receptors α and β, macrophage colony-stimulating factor (M-CSF) receptor, and the flt3 receptor. All members of this RTK family contain five immunoglobulin-like (Ig) domains in their extracellular ligand-binding domains followed by a single transmembrane domain and a cytoplasmic tyrosine kinase domain interrupted by a large kinase insert. Like other RTKs, SCF induces dimerization of c-kit followed by trans-autophosphorylation of the cytoplasmic protein tyrosine kinase domain, leading to subsequent recruitment of signaling proteins, tyrosine phosphorylation of substrates, and activation of multiple signaling pathways (5, 6).

SCF exists naturally as membrane-anchored and soluble isoforms as a result of alternative RNA splicing and proteolytic processing (7, 8). The soluble form of SCF has 165 amino acids, but its receptor-binding core has been mapped to the first 141 residues (9). SCF functions as a noncovalent homodimer, but under physiological conditions, the majority of SCF exists as a monomer (10). Dimerization of SCF is a dynamic process, and it may play a regulatory role in the control of SCFR binding affinity and receptor activation. In this report, we present the crystal structure of the SCF dimer. The structure of each protomer is a short chain four-helix bundle. The two protomers interact head-to-head to form an elongated, slightly bent dimer, and the dimeric interface is formed by extensive polar as well as nonpolar interactions. Determination of the structure of SCF is an important step in achieving a complete understanding of the structure of SCF in complex with SCFR and elucidation of its mechanism of action.

Materials and Methods

Protein Expression, Refolding, and Purification. SCF (residues 1–141) was expressed in *Escherichia coli* as inclusion bodies as described previously (11). Inclusion bodies from 1 liter of bacterial culture were dissolved in 25–30 ml of 6 M guanidine hydrochloride solution. After the solution became clear, DTT was added to a final concentration of 40 mM and the mixture was incubated at 37°C for 30 min. The resulting solution was diluted into 4 liters of buffered solution (10 mM Tris·HCl, pH 8.5) and allowed to stand overnight. Refolded protein was purified by ion-exchange chromatography.

Crystallization and Data Collection. Crystals of SCF were grown by vapor diffusion at 20°C by using the hanging-drop method. Two crystal forms are produced. Orthorhombic crystals were grown by mixing 2 μl of protein sample (≈15–20 mg/ml) with 2 μl of reservoir consisting of ≈25–30% PEG 400, 0.25 M $CaCl_2$, and 0.1 M Hepes (pH 7.0). Addition of 1 mM $SmCl_3$ to the protein solution produced the monoclinic crystals (a = 36.15 Å, b = 87.53 Å, c = 79.43 Å, β = 97.76°) that were used in the structure determination (Table 1).

Crystals for data collections were flash-frozen in liquid propane directly from the crystallization drops. Initial characterization of the SCF crystals was done at synchrotron beamlines X26C and X4A of the National Synchrotron Light Source, Brookhaven National Laboratory, and the final data collection was done at Argonne National Laboratory Structural Biology Center beamline 19-ID at the Advanced Photon Source. All data were processed by using DENZO, and the intensities were reduced and scaled by using SCALEPACK (12).

Structure Determination, Model Building, and Refinement. A molecular replacement attempt with the data collected from the orthorhombic crystals by using a model built from the C_α atom positions of the human M-CSF (13) was not successful. Data used for the structure determination were collected from the monoclinic crystals at wavelengths 1.03 Å and 1.55 Å, which are not at the absorption edge of Sm. The anomalous signal was clear from Patterson difference maps. The heavy metal position refinement and phasing were done with PHASES (14). Three Sm sites were used for phasing, whereas four Sm atoms were placed

Abbreviations: SCF, stem cell factor; SCFR, SCF receptor; RTK, receptor tyrosine kinase; PDGF, platelet-derived growth factor; M-CSF, macrophage colony-stimulating factor.

Data deposition: The atomic coordinates have been deposited in the Protein Data Bank, www.rcsb.org (PDB ID code 1EXZ).

¶To whom reprint requests should be addressed at: Departments of Pharmacology and Biochemistry and Skirball Institute, NYU Medical Center, 550 First Avenue, New York, NY 10016. E-mail: g967758@med.nyu.edu or kong@saturn.med.nyu.edu.

The publication costs of this article were defrayed in part by page charge payment. This article must therefore be hereby marked "*advertisement*" in accordance with 18 U.S.C. §1734 solely to indicate this fact.

Table 1. X-ray diffraction data

Data collection		
Wavelength, Å	1.03	1.55
Resolution range, Å	40–2.3	40–2.3
R_{merge}	5.8 (25.0)	7.5 (27.0)
I/σ	29	30
Completeness, %	99.5	99.5
Figure of merit	0.44	
Refinement		
Resolution, Å	40–2.3	
R_{work}	22.4	
R_{free}	29.4	
No. of reflections		
Working set	19,321	
Test set	2,133	
No. of heteroatoms		
Solvent	132	
Ion	6	
Other	Tris	
Deviations from ideal geometry		
Bond lengths, Å	0.007	
Bond angles, °	1.22	
Average *B* factors		
Protein	44.13	
Solvent	44.5	

in the final model. Only short pieces of helices were visible from the initial solvent-flattened electron density map, and they were built into the density with program O (15). Repeated cycles of model building and solvent flattening combined with partial structures were performed until most of all four molecules in the asymmetric unit were built. Subsequent refinements were carried out against the lower-energy (wavelength of 1.03 Å) diffraction data with Crystallography and NMR System (CNS) (16). Refinement progress was monitored with the R_{free} value, using a 10% randomly selected test data set, and residue positions were adjusted against $2F_o - F_c$ electron density maps. Table 1 gives the statistics of the final model, which contains 132 solvent molecules, four samarium ions, two calcium ions, and one Tris molecule.

Figure Preparation. Figs. 1*A*, 2*A*, and 3 were constructed by MOLSCRIPT and RASTER3D (45, 46). Fig. 2*B* was created by O (15), and Fig. 4 *A* and *C,* by GRASP (47).

Results and Discussion

Structure Determination. The functional core of SCF, composed of amino acids 1–141 (9), was expressed in *E. coli* as inclusion bodies and refolded by denaturation and renaturation. Two crystal forms diffracting to better than 2-Å resolution were obtained (see *Materials and Methods*). Only the monoclinic crystals containing samarium ions were used for structure determination. The structure was determined by using anomalous scattering differences of samarium ions in the crystal at two wavelengths and refined to 2.3 Å (Table 1). There are four molecules in each asymmetric unit, and the initial experimental electron density clearly showed the four-helix bundle and two β-strands in the molecules. The connecting loops, as well as the N-terminal and C-terminal regions, were built from $2F_o - F_c$ maps. The final model contains four samarium ions, two of which play a role in holding flexible loops. In addition, two calcium ions, and one Tris moiety were built into the structure.

General Features of the Structure. Although there are four SCF protomers in the crystallographic asymmetric unit, the biological dimer is unmistakably recognizable. The four protomers are

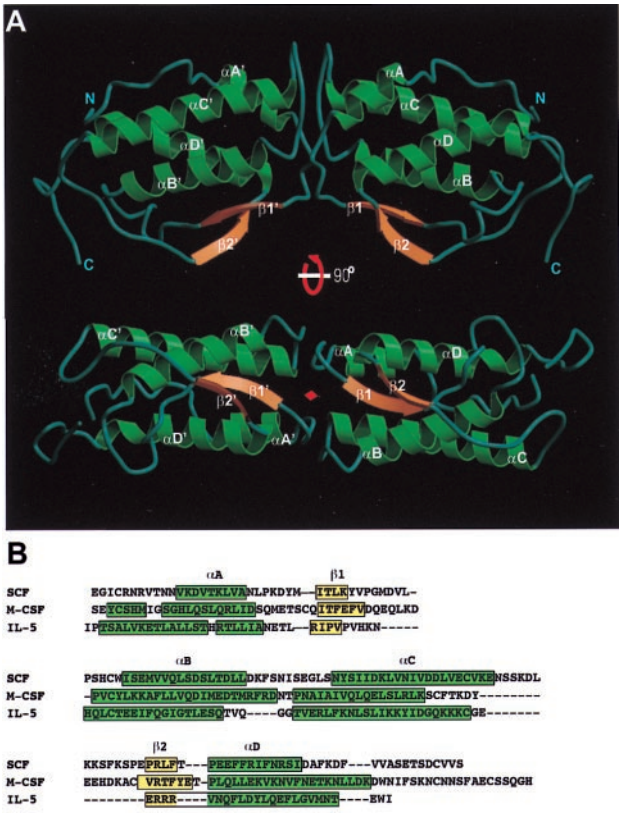

Fig. 1. Overall structure of SCF and its relationship with other cytokines. (*A*) Ribbon representation of the SCF structure, in two views related by a rotation of approximately 90°. The termini and secondary structures are labeled; the β-strands are rendered as orange arrows, the helices as green ribbons, and the loop regions as gray tubes. The twofold axis is marked with a red diamond. (*B*) Sequence alignment based on secondary structures of SCF, M-CSF, and IL-5. Secondary structure assignments for M-CSF and IL-5 are from the Protein Data Bank. β-Strands are yellow and helices are bright green.

superimposable except for the N-terminal and C-terminal loop regions. These loops are flexible and adopt multiple conformations in the four molecules in the asymmetric unit. The protomers in the biological dimer are packed head-to-head with almost perfect *C*2 symmetry (Fig. 1*A*). The dimer bends approximately 30° toward the side of the β-strands, resulting in an elongated shape with approximate dimensions of 87 Å × 32 Å × 25 Å.

The overall topology of an SCF protomer displays an antiparallel four-helix bundle fold (Fig. 1*A*), in a manner similar to other short-chain helix cytokines (17). The helices run up-up-down-down, with two crossing β-strands wrapped on one side. The side chains of the hydrophobic residues of the four helices pack in the core of each monomer. Cys-4 and Cys-89 as well as Cys-43 and Cys-138 form two intramolecular disulfide pairs. Both disulfide bonds are located at one end (tail) of each protomer away from the dimer interface. The Cys-4–Cys-89 disulfide bond is more exposed than the Cys-43–Cys-138 disulfide bond. The latter is wrapped by the side chains of Val-39, Leu-98, Pro-40, and His-42. This wrapping probably explains why the Cys-4–Cys-89 disulfide bond is more susceptible to chemical reduction than is the Cys-43–Cys-138 bond (18).

Comparison with Other Growth Factors. SCF belongs to the short-chain helical cytokine family (17, 19), but its resemblance to the other cytokines is limited to the overall fold. The primary structures exhibit very weak similarity, and sequences can be

aligned only by comparison of the secondary structures (Fig. 1*B*). The structure of SCF is most similar to the structure of M-CSF (13). The core four helix bundles of the two proteins superimpose relatively well, with rms deviation of 1.98 Å for the C_α atoms. However, upon superimposition of the helices, the two β-strands deviate significantly. Two loops in SCF, residues 29–41 and residues 90–98, extrude more than those of M-CSF. At the dimer interface, the SCF loop from residue 61 to residue 72 also extrudes further away from the core and packs against the same loop from the second protomer. This structure results in more contact between the two protomers of SCF as compared with the contact between the two M-CSF protomers (see below). Furthermore, M-CSF is a covalent homodimer linked by an intermolecular disulfide bond, whereas SCF is a noncovalent homodimer. flt3 ligand is also a noncovalent homodimer, but it has an extra intramolecular disulfide bond, as does M-CSF (20, 21). Nevertheless, the structure of flt3 ligand can be predicted with reasonable confidence on the basis of the crystal structures of SCF described in this report and the previously described crystal structure of M-CSF (20).

The Dimer Interface. In contrast to the disulfide-linked PDGF and M-CSF homodimers, two other ligands of the same family of RTKs, SCF functions as a noncovalent homodimer. It has been shown that the bivalency of SCF is the sole driving force responsible for dimerization of the extracellular ligand-binding domains of c-kit (22). Hence analyses of the molecular interactions that control SCF-dimer formation are critical for understanding the mechanism of activation of c-kit. The x-ray structure of SCF shows that there are extensive interactions between the two SCF protomers, with approximately 1,700-Å^2 surface area buried upon dimerization (calculated with a probe of radius 1.4 Å) (23). This buried surface area accounts for about 20% of the total surface of each individual protomer, and is twice that of the 850-Å^2 buried surface area of the disulfide-linked M-CSF dimer (13).

The SCF dimer interface is composed of loops between αA and β1, αB and αC, and can also be divided into three layers (Fig. 2*A*). The bottom layer at the side of the β-strands takes part in hydrophobic interactions. Side chains from Tyr-26, Pro-23, Phe-63, and Leu-22 from one protomer pack against corresponding side chains from the other protomer, with Tyr-26–Asp-25′ and Tyr-26′–Asp-25 forming a hydrogen bond circle (Fig. 2*B*). These intermolecular hydrogen bond pairs replace the intermolecular disulfide bond between the two M-CSF protomers (19, 24). Sequence alignment shows that this Tyr-Asp pair is preserved in flt3 ligand, the third member of this family of cytokines, which also forms dimers by noncovalent interactions (21). At the core of the interface, the side chains of four asparagine residues (Asn-72 and Asn-21 from both protomers) form hydrogen bonds among themselves as well as via a water molecule (Fig. 2*A*). This well-coordinated water molecule forms hydrogen bonds, with an average bond length of 2.7 Å, with the two carbonyl oxygen atoms of the two symmetry-related Asn-21 residues. The top layer involves interactions between loop αB-αC of one protomer against that of the other protomer. These two loops serve as a wedge to bend the dimer toward the side of the β-strands. In addition to a dozen hydrogen bonds formed between the two protomers, there are four possible salt bridges, Lys-17–Glu-68′, Lys-24–Asp-61′, and their symmetry-related counterparts.

Dimerization of SCF is sensitive to pH and salt concentration changes (25). This property is likely due to the fact that the interface is formed in part by polar interactions via salt bridges at the periphery and by water molecule-mediated hydrogen bonds among buried polar residues at the core of the interface. In an attempt to identify residues that play a role in SCF dimerization, a Phe-63 → Cys mutant was generated and characterized for receptor-binding activity (10). It was demonstrated

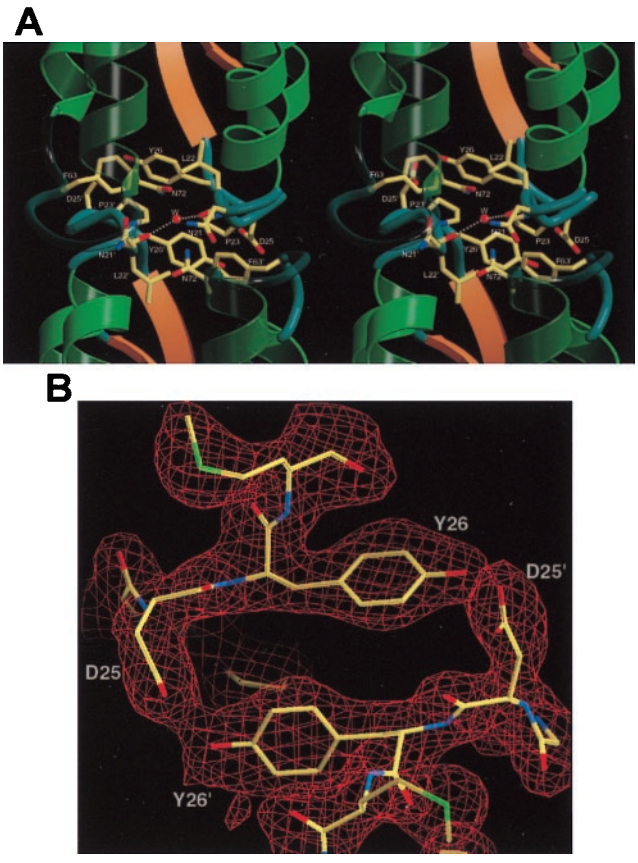

Fig. 2. Dimer interface. (*A*) Stereoview of the dimer interface. For clarity, only side chains of residues at the core of the interface are shown. Color coding of the secondary structures is the same as in Fig. 1*A*. (*B*) $2F_o - F_c$ electron density, contoured at 1.2σ, for the hydrogen bond circle of Tyr-26 and Asp-25′ at the dimer interface.

that this mutation led to the formation of a covalent SCF dimer. However, the mutant SCF dimer was biologically inactive. The structure of the SCF interface provides a plausible explanation for the lack of activity of this mutant (Fig. 2*A*). In the structure, the shortest distance between the side chains of the two symmetry-related Phe-63 residues is about 8 Å, with the well-coordinated water molecule between them. It is impossible to create a disulfide bond between these two residues without disrupting the secondary and tertiary structures of the SCF dimer.

Domain Swapping and the Covalent Dimer of SCF. Recombinant SCF is expressed in *E. coli* as inclusion bodies in a denatured form, and an active SCF protein is produced by a procedure involving refolding and oxidation. A small fraction of the refolded-oxidized protein is a covalent disulfide-linked form of SCF (18, 26). Interestingly, the covalent SCF dimer bound to c-kit with slightly reduced affinity but was more potent in stimulation of hematopoietic cells (25). Comparison of the secondary and tertiary structures by spectroscopic methods demonstrated that the covalent dimer is indistinguishable from the noncovalent dimer (18). Surprisingly, the disulfide linkages of the covalent dimer were found to be identical to those in the noncovalent dimer except that the disulfide linkages in the variant protein were intermolecular. That is, Cys-4 and Cys-43 from one protomer form disulfide bonds with Cys-89 and Cys-138, respectively, of the second protomer. It was thus proposed that the covalent dimer could be formed by a three-dimensional domain swapping of

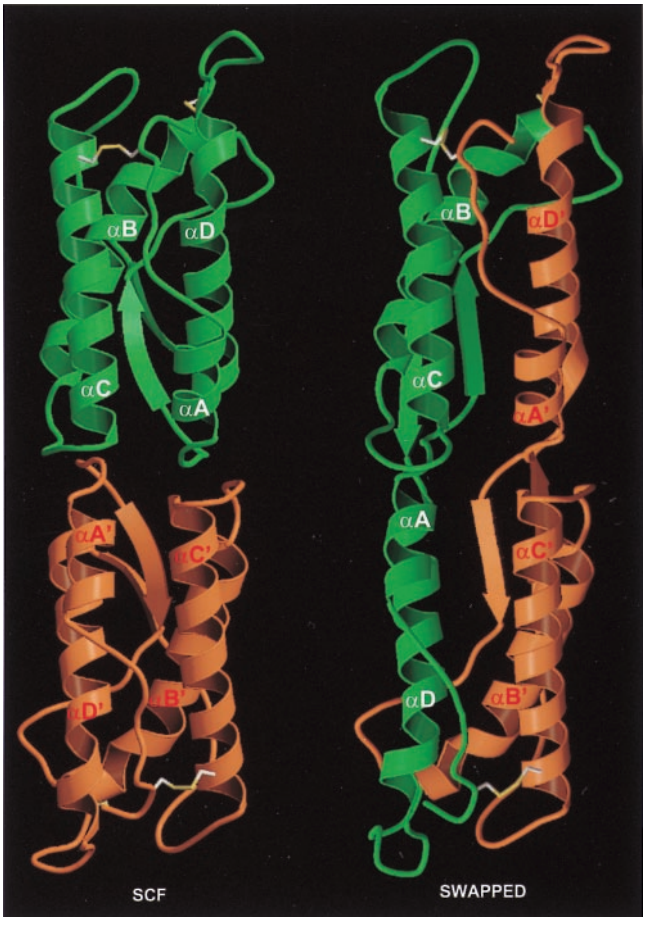

Fig. 3. Model of covalent SCF dimer. The noncovalent (native) dimer is on the left and a model for the covalent SCF dimer is on the right. Each protomer is colored either orange or green. The disulfide bonds are shown in ball-and-stick with sulfur atoms colored yellow.

helices αA and αD between the two monomers (18). A close examination of the structure of SCF shows that the *C*2 symmetry of the dimer may allow these helices to be swapped between the protomers while preserving the overall structure and surface at the tails of each protomer. Fig. 3 shows a model generated by swapping helices αA and αD between the two protomers. Interestingly, the interactions at the core between the helices from the original dimer are preserved in the swapped model, whereas the loops around the *C*2 axis and the orientation of the strands have to be adjusted. The disulfide pairs are identical in the two forms except that they are intramolecular in the noncovalent dimer and intermolecular in the covalent dimer. It is worth noting that other four-helix bundle cytokines such as IL-5, IL-10, and IFN-β form similar covalent interdigitated dimers naturally (27). In IL-5, helix αD and strand β2 of one protomer, together with helices αA, αB, and αC and strand β1 from the other protomer, form one domain of the two-domain dimer. Indeed, because of the symmetric nature of the structure, it was possible to generate monomeric IL-5 mutants (28–30). By the same token, new types of interdigitated covalent SCF dimers could be formed by introducing mutations in the loops between helix αA and strand β1 and between β2 and helix αD that favor the covalent dimer structure. These similarities in fold and dimeric symmetry among the helical cytokines probably reflect their common evolutionary origin.

Three-dimensional domain swapping is considered to be a general mechanism for the regulation of oligomer assembly: that is, oligomers are formed from stable monomers by exchanging domains during evolution or under controlled laboratory conditions (27). Under normal physiological conditions, the majority of soluble SCF exists as monomers (10). The balance between SCF monomers and dimers may be linked to the physiological requirement for activation of c-kit expressed on target cells *in vivo*. However, for therapeutic purposes, the more potent disulfide-linked dimer is preferred because it can be administered at low doses to avoid significant mast cell activation while stimulating hematopoietic recovery (26). With the detailed structural information available, it may now be possible to design novel SCF variants with increased therapeutic potency.

A Receptor-Binding Region on SCF. SCF dimers bind soluble or membrane forms of c-kit with high affinity and specificity (22). The binding of SCF to c-kit was analyzed by biochemical methods, by employing site-directed mutagenesis and by epitope mapping with site-specific anti-c-kit antibodies. It was demonstrated that deletions of residues 1–3 from the N terminus reduced the binding of SCF to c-kit by approximately 50% (9). Deletion of Cys-4 inactivated SCF, whereas deletion of Cys-138 and additional residues from the C terminus only compromised SCF activity. Moreover, an SCF double mutant, Cys-43 → Ala and Cys-138 → Ala, which eliminates one pair of disulfide bonds, resulted in a partially active SCF as well. These experiments demonstrated that the N terminus of SCF and the integrity of the Cys-4–Cys-89 disulfide bond are crucial for full SCF activity.

By analyzing the activities of a variety of SCF/M-CSF chimeric proteins, it has been shown that Arg-121, Asp-124, Lys-127, and Asp-128 are essential for SCF activity (8). Moreover, by using antibodies that neutralize different epitopes on SCF, it was demonstrated that the regions flanked by amino acids 61–65 and 91–95 are also essential for SCF activity (31). In general, the regions mapped by biochemical methods are located in close proximity at the tail region of each SCF protomer. This region contains a deep crevice at the end of αC formed by side chains of the hydrophobic residues Phe-102, Leu-98, Pro-34, and Tyr-32, and by the Cys-43–Cys-138 disulfide bridge (Fig. 4*A*). Next to the crevice, there are three charged patches: a positively charged patch (Arg-5, Arg-7, and Lys-127) followed by a negatively charged patch (Asp-84, Asp-85, Glu-88, and Glu-92) and then by an additional positively charged patch (Lys-91, Lys-99, Lys-100, and Lys-103). Fig. 4*A* shows the locations of the positively charged (blue) and negatively charged (red) patches as well as the hydrophobic crevice (yellow). This surface may function as a receptor-binding site with the charged interactions providing anchor and specificity for ligand/receptor interactions and the hydrophobic interactions providing enthalpy to complex formation.

While human and rodent SCFs are highly conserved, the charged patches that may function as part of receptor binding regions are quite divergent (Fig. 4*B*). Arg-5 and Arg-7 in the first positively charged patch of the human SCF are replaced by glycine and proline residues in rodents, respectively. In the second positively charged patch, Lys-100 and Lys-91 are replaced by glutamate residues in both mouse and rat. These changes could account for the difference in the binding affinity of human and murine SCF to the human c-kit (32).

Natural and CHO-cell-derived recombinant SCF are glycosylated on multiple asparagine, serine, and threonine residues (33). The receptor-binding properties of glycosylated SCF are consistent with the assignment of SCFR-binding region shown in Fig. 4*A*. There are four putative asparagine glycosylation sites in the functional core of SCF: Asn-65, Asn-72, Asn-93, and Asn-120. Asn-72 is not glycosylated, probably because its side chain is buried in the dimer interface. However, the side chains of Asn-120, Asn-65, and Asn-93 remain accessible to the solvent in the structure and are indeed glycosylated to different extents.

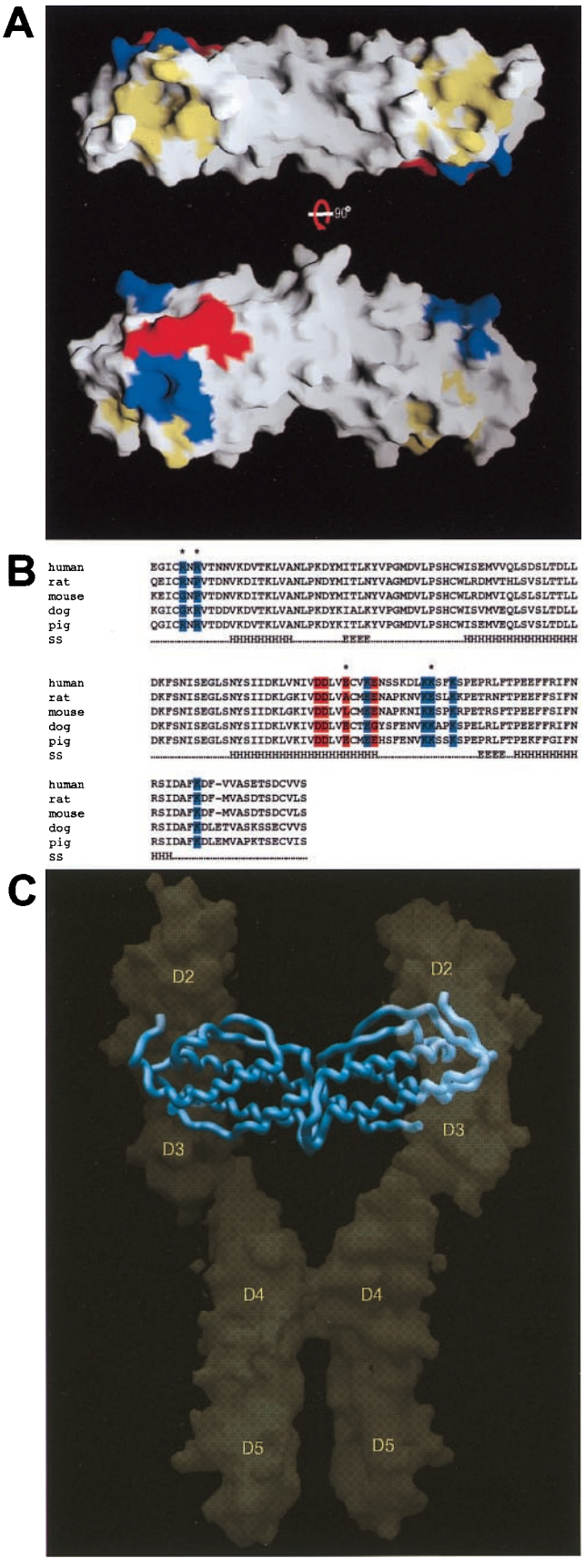

Fig. 4. A potential binding site on SCF for c-kit and a model of SCF·SCFR complex. (*A*) Molecular surface of SCF and proposed c-kit binding regions, in two views related by a rotation of approximately 90°. A hydrophobic crevice at both tails is colored yellow. Two basic patches are colored blue, and the acidic patch is colored red. (*B*) Sequence alignments of human, rat, mouse, dog, and pig SCFs. Residues of the acidic patch are colored red and residues of the two basic patches are colored blue. Asterisks mark amino acid residues that are altered in rodents. The secondary structures (SS) are marked below the sequences with H representing helices and E representing β-strands. (*C*) Proposed model of the SCF in complex with Ig-like domains 2–5 of the extracellular domain of c-kit (labeled D2 to D5). SCF dimer is represented in a worm model, and the c-kit model is represented by a molecular surface.

Asn-120 is always glycosylated, but this does not affect the binding of SCF to c-kit. In contrast, Asn-65 and Asn-93 are glycosylated in some, but not all, SCF molecules. Importantly, glycosylation of these asparagine residues has an adverse effect on SCF binding to SCFR (32). The structure provides possible explanations for the adverse effect of glycosylation of these residues on the activity of SCF. The glycosylation of Asn-93 may hinder SCF binding to c-kit, as this residue is located very close to the acidic patch and to the hydrophobic crevice. On the other hand, Asn-65 is located close to the dimer interface, and glycosylation of this residue may interfere with SCF dimerization.

A Model for the SCF·SCFR Complex. The extracellular ligand-binding domains of several RTKs contain multiple Ig-like domains. For instance, the extracellular domains of the fibroblast growth factor (FGF) receptor (FGFR) contain three Ig-like domains, whereas the extracellular domain of the PDGF-receptor family, to which c-kit belongs, is composed of five Ig-like domains. Similarly, the extracellular domain of the vascular endothelial growth factor (VEGF) receptor (VEGFR) contains seven Ig-like domains (34). Although the ligands of these receptors are very diverse, the ligand-binding regions in these three families of receptors have been mapped to Ig-like domains 2 and 3 (22, 35, 36). The determination of the structures of the ligand-binding domains of FGF and VEGF receptors demonstrated that FGF and VEGF bind differently to their respective receptors. In the FGF·FGFR complex, the two receptors are packed side-by-side to one face and the ligands occupy the second face. On the other hand, the two VEGFRs bind to the far ends of the VEGF dimer, creating an H-shaped complex with the ligand representing the cross bar. Because SCF functions as a dimer, we expect that SCF binding to c-kit resembles the structure of the VEGF·VEGFR complex (35). Using the structure of FGFR as a template, we have built a model for Ig-like domains 2–3 as well as 4–5 of c-kit. We then docked Ig-like domains 2 and 3 to the proposed SCF binding surface, adopting the mode of FGFR binding to FGF2 (36). In addition, we have adjusted the orientation of Ig-like domains 4 and 5 to allow for interactions between domain 4 in the complex as suggested by biochemical studies (37) (Fig. 4*C*).

Conclusions

c-kit belongs to the family of RTKs that includes M-CSF receptor, PDGF receptor α, PDGF receptor β, and flt3. Comparison of their primary structures shows that these RTKs are much more conserved than their cognate ligands. Indeed, the structures of PDGF-A and PDGF-B are dramatically different from the structures of M-CSF and SCF and probably also flt3 ligand. The similarity of the RTKs is also reflected in the chromosomal localizations of their human and murine genes (38). It is thought that this family of RTKs has evolved from a common ancestral gene that has undergone several gene-duplication events. It is worth pointing out that RTKs that bind to and are activated by ligands having structures of four helix bundles (i.e., M-CSF, SCF, and flt3 ligand) are primarily involved in the control of hematopoiesis, whereas other members of this family of RTKs exhibit a broader expression pattern and

are involved in the regulation of growth and development of several tissues and organs.

SCF has been tested extensively in both animals and humans because of its ability to promote hematopoietic recovery (39–43). It has been demonstrated that SCF treatments produce an increase in the number of peripheral blood neutrophils and hematopoietic progenitor cells and modest rises in the numbers of platelets and lymphocytes (44). SCF, alone or in combination with other cytokines, is used to reduce the hematological damage of chemotherapy. In a separate clinical trial, SCF has also been proven to be effective in enhancing the ability of granulocyte colony-stimulating factor to mobilize peripheral blood hematopoietic progenitor and stem cells. It is believed that these cells can be transplanted to reconstitute the hematopoietic system in patients receiving bone marrow ablative therapy (44). In view of these clinical observations, determination of the three-dimensional structure of SCF will facilitate the determination of the structure of SCF in complex with the extracellular domain of c-kit, and will enable the design and production of more potent forms of therapeutic SCF analogues.

We thank Dieter Schneider (beamline X26C) and Craig Ogata (beamline X4A) for help with data collection at their beamlines, and Arnold Lee for help with the final data collection.

1. Galli, S. J., Zsebo, K. M. & Geissler, E. N. (1994) *Adv. Immunol.* **55,** 1–96.
2. Williams, D. E., Eisenman, J., Baird, A., Rauch, C., Van Ness, K., March, C. J., Park, L. S., Martin, U., Mochizuki, D. Y., Boswell, H. S., *et al.* (1990) *Cell* **63,** 167–174.
3. Zsebo, K. M., Williams, D. A., Geissler, E. N., Broudy, V. C., Martin, F. H., Atkins, H. L., Hsu, R. Y., Birkett, N. C., Okino, K. H., Murdock, D. C., *et al.* (1990) *Cell* **63,** 213–224.
4. Huang, E., Nocka, K., Beier, D. R., Chu, T. Y., Buck, J., Lahm, H. W., Wellner, D., Leder, P. & Besmer, P. (1990) *Cell* **63,** 225–233.
5. Lemmon, M. A. & Schlessinger, J. (1994) *Trends Biochem. Sci.* **19,** 459–463.
6. Hunter, T. (2000) *Cell* **100,** 113–127.
7. Lu, H. S., Clogston, C. L., Wypych, J., Fausset, P. R., Lauren, S., Mendiaz, E. A., Zsebo, K. M. & Langley, K. E. (1991) *J. Biol. Chem.* **266,** 8102–8107.
8. Matous, J. V., Langley, K. & Kaushansky, K. (1996) *Blood* **88,** 437–444.
9. Langley, K. E., Mendiaz, E. A., Liu, N., Narhi, L. O., Zeni, L., Parseghian, C. M., Clogston, C. L., Leslie, I., Pope, J. A., Lu, H. S., *et al.* (1994) *Arch. Biochem. Biophys.* **311,** 55–61.
10. Hsu, Y. R., Wu, G. M., Mendiaz, E. A., Syed, R., Wypych, J., Toso, R., Mann, M. B., Boone, T. C., Narhi, L. O., Lu, H. S. & Langley, K. E. (1997) *J. Biol. Chem.* **272,** 6406–6415.
11. Langley, K. E., Wypych, J., Mendiaz, E. A., Clogston, C. L., Parker, V. P., Farrar, D. H., Rozwarski, D. A., Gronenborn, A. M., Clore, G. M., Bazan, J. F., *et al*. (1994) *Structure* **2,** 159–173.
12. Otwinowski, Z. & Minor, W. (1997) *Methods Enzymol.* **276,** 307–326.
13. Pandit, J., Bohm, A., Jancarik, J., Halenbeck, R., Koths, K. & Kim, S. H. (1992) *Science* **258,** 1358–1362.
14. Furey, W. & Swaminathan, S. (1997) *Methods Enzymol.* **277,** 590–620.
15. Jones, T. A., Zou, J. Y., Cowan, S. W. & Kjeldgaard, M. (1991) *Acta Crystallogr. A* **47,** 110–119.
16. Brunger, A. T., Adams, P. D., Clore, G. M., DeLano, W. L., Gros, P., Grosse-Kunstleve, R. W., Jiang, J. S., Kuszewski, J., Nilges, M., Pannu, N. S., *et al.* (1998) *Acta. Crystallogr. D* **54,** 905–921.
17. Rozwarski, D. A., Gronenborn, A. M., Clore, G. M., Bazan, J. F., Bohm, A., Wlodawer, A., Hatada, M. & Karplus, P. A. (1994) *Structure* **2,** 159–173.
18. Lu, H. S., Jones, M. D., Shieh, J. H., Mendiaz, E. A., Feng, D., Watler, P., Narhi, L. O. & Langley, K. E. (1996) *J. Biol. Chem.* **271,** 11309–11316.
19. Bazan, J. F. (1991) *Cell* **65,** 9–10.
20. Lyman, S. D., James, L., Vanden Bos, T., de Vries, P., Brasel, K., Gliniak, B., Hollingsworth, L. T., Picha, K. S., McKenna, H. J., Splett, R. R., *et al.* (1993) *Cell* **75,** 1157–1167.
21. Hannum, C., Culpepper, J., Campbell, D., McClanahan, T., Zurawski, S., Bazan, J. F., Kastelein, R., Hudak, S., Wagner, J., Mattson, J., *et al.* (1994) *Nature (London)* **368,** 643–648.
22. Lemmon, M. A., Pinchasi, D., Zhou, M., Lax, I. & Schlessinger, J. (1997) *J. Biol. Chem.* **272,** 6311–6317.
23. Lee, B. & Richards, F. M. (1971) *J. Mol. Biol.* **55,** 379–400.
24. Broudy, V. C. (1997) *Blood* **90,** 1345–1364.
25. Lu, H. S., Chang, W. C., Mendiaz, E. A., Mann, M. B., Langley, K. E. & Hsu, Y. R. (1995) *Biochem. J.* **305,** 563–568.
26. Nocka, K. H., Levine, B. A., Ko, J. L., Burch, P. M., Landgraf, B. E., Segal, R. & Lobell, R. (1997) *Blood* **90,** 3874–3883.
27. Bennett, M. J., Schlunegger, M. P. & Eisenberg, D. (1995) *Protein Sci.* **4,** 2455–2468.
28. Dickason, R. R. & Huston, D. P. (1996) *Nature (London)* **379,** 652–655.
29. Dickason, R. R., English, J. D. & Huston, D. P. (1996) *J. Mol. Med.* **74,** 535–546.
30. Edgerton, M. D., Graber, P., Willard, D., Consler, T., McKinnon, M., Uings, I., Arod, C. Y., Borlat, F., Fish, R., Peitsch, M. C., *et al*. (1997) *J. Biol. Chem.* **272,** 20611–20618.
31. Mendiaz, E. A., Chang, D. G., Boone, T. C., Grant, J. R., Wypych, J., Aguero, B., Egrie, J. C. & Langley, K. E. (1996) *Eur. J. Biochem.* **239,** 842–849.
32. Lu, H. S., Clogston, C. L., Wypych, J., Parker, V. P., Lee, T. D., Swiderek, K., Baltera, R. F., Jr., Patel, A. C., Chang, D. C., Brankow, D. W., *et al.* (1992) *Arch. Biochem. Biophys.* **298,** 150–158.
33. Arakawa, T., Langley, K. E., Kameyama, K. & Takagi, T. (1992) *Anal. Biochem.* **203,** 53–57.
34. Fantl, W. J., Johnson, D. E. & Williams, L. T. (1993) *Annu. Rev. Biochem.* **62,** 453–481.
35. Wiesmann, C., Fuh, G., Christinger, H. W., Eigenbrot, C., Wells, J. A. & de Vos, A. M. (1997) *Cell* **91,** 695–704.
36. Plotnikov, A. N., Schlessinger, J., Hubbard, S. R. & Mohammadi, M. (1999) *Cell* **98,** 641–650.
37. Blechman, J. M., Lev, S., Barg, J., Eisenstein, M., Vaks, B., Vogel, Z., Givol, D. & Yarden, Y. (1995) *Cell* **80,** 103–113.
38. Rousset, D., Agnes, F., Lachaume, P., Andre, C. & Galibert, F. (1995) *J. Mol. Evol.* **41,** 421–429.
39. Medlock, E. S., Migita, R. T., Trebasky, L. D., Housman, J. M., Elliott, G. S., Hendren, R. W., Deprince, R. B. & Greiner, D. L. (1992) *Dev. Immunol.* **3,** 35–44.
40. Zsebo, K. M., Smith, K. A., Hartley, C. A., Greenblatt, M., Cooke, K., Rich, W. & McNiece, I. K. (1992) *Proc. Natl. Acad. Sci. USA* **89,** 9464–9468.
41. Andrews, R. G., Bensinger, W. I., Knitter, G. H., Bartelmez, S. H., Longin, K., Bernstein, I. D., Appelbaum, F. R. & Zsebo, K. M. (1992) *Blood* **80,** 2715–2720.
42. Morstyn, G., Glaspy, J., Shpall, E. J., LeMaistre, F., Briddell, R., Menchaca, D., Lill, M., Jones, R. B., Tami, J., Brown, S., *et al.* (1994) *J. Hematother.* **3,** 353–355.
43. Brandt, J. E., Bhalla, K. & Hoffman, R. (1994) *Blood* **83,** 1507–1514.
44. Nicola, N. A. & Hilton, D. J. (1998) *Adv. Protein Chem.* **52,** 1–65.
45. Kraulis, P. J. (1991) *J. Appl. Crystallogr.* **24,** 946–950.
46. Merrit, E. A. & Bacon, D. J. (1991) *Methods Enzymol.* **202,** 505–524.
47. Nicolls, A., Sharp, K. A. & Honog, B. (1991) *Proteins* **11,** 281–296.